Rhythmic modulation of visual perception by continuous rhythmic auditory stimulation

Anna-Katharina R. Bauer*[1,2], Freek van Ede[2,3], Andrew J. Quinn[1,2], & Anna C. Nobre[1,2]

1. *Department of Experimental Psychology, Brain and Cognition Lab, University of Oxford, OX2 6GG, UK*
2. *Oxford Centre for Human Brain Activity, Wellcome Centre for Integrative Neuroimaging, Department of Psychiatry, University of Oxford, Oxford, UK*
3. *Institute for Brain and Behavior Amsterdam, Department of Experimental and Applied Psychology, Vrije Universiteit Amsterdam, 1081BT, The Netherlands*

**Corresponding author*

Highlights

- cross-modal influences are mediated by the synchronisation of neural oscillations
- visual performance fluctuates in line with the phase of a frequency-modulated sound
- cross-modal entrainment of neural activity predicts fluctuation in visual performance
- cross-modal entrainment organises perception of multisensory stimuli

Abstract

At any given moment our sensory systems receive multiple, often rhythmic, inputs from the environment. Processing of temporally structured events in one sensory modality can guide both behavioural and neural processing of events in other sensory modalities, but how this occurs remains unclear. Here, we used human electroencephalography (EEG) to test the cross-modal influences of a continuous auditory frequency-modulated (FM) sound on visual perception and visual cortical activity. We report systematic fluctuations in perceptual discrimination of brief visual stimuli in line with the phase of the FM sound. We further show that this rhythmic modulation in visual perception is related to an accompanying rhythmic modulation of neural activity recorded over visual areas. Importantly, in our task, perceptual and neural visual modulations occurred without any abrupt and salient onsets in the energy of the auditory stimulation and without any rhythmic structure in the visual stimulus. As such, the results provide a critical validation for the existence and functional role of cross-modal entrainment and demonstrates its utility for organising the perception of multisensory stimulation in the natural environment.

Keywords: multisensory perception, neural entrainment, rhythmic attentional sampling, cross-modal influences, frequency modulated sounds, EEG

Introduction

Our sensory environment is filled with rhythmic structure to which neural activity can become synchronised. This synchronisation of neural activity and rhythmic structures in the environment is often referred to as "neural entrainment", a process by which two self-sustained oscillations become coupled via phase and/or frequency adjustment [1–3]. Low-frequency neural entrainment has been suggested as an important mechanism for enabling cross-modal influences by facilitating the transfer of information across sensory modalities [4–8].

To date, studies that have investigated cross-modal influences of auditory rhythms on visual perception have relied on rhythmic auditory streams with identifiable onsets and offsets, such as individual transient events (tones) or amplitude modulations [1,5,8–14]. However, such onsets may cause cross-modal influences simply because they are salient or because the individual events that make up such rhythms may repeatedly evoke cross-modal phase-resets of neural activity [15–23]. Thus, any observed behavioural or neural modulations may not directly or only partly entail true "entrainment" of neural activity [24–29]. To bypass this complication when interpreting cross-modal influences of auditory rhythmic stimulation on visual performance and neural activity, we used a continuous auditory stimulus for which periodicity was conveyed via frequency-modulation (FM). The advantage of using an FM-sound is that this type of auditory stimulation conveys clear "rhythmicity" in the perception of the listener, while keeping the overall "energy" (amplitude) of the sound constant over time (as shown in Figure 1A).

In previous uni-modal work, we and others have demonstrated that a continuous auditory FM stimulation can profoundly impact the ability to detect near-threshold auditory targets embedded in the auditory stream, such that detection performance varies systematically with the phase of the FM-sound [30–33]. Here, we test whether a continuous FM-sound can also influence perception and neural activity *cross-modally* to modulate visual perception and related cortical activity.

To test for cross-modal auditory-to-visual influences, participants (N = 28) identified the orientation of a briefly presented visual Gabor grating, either rotated 45- or 135-degree, embedded within a two-second 3-Hz frequency-modulated (FM) stimulus (Figure 1A; Sound) while electroencephalography (EEG) was recorded. Critically, visual targets were presented at different times, relative to the phase of the continuous FM auditory stimulation (see Figure 1B: visual target times; Video). We predicted that ongoing neural oscillations in auditory cortices would entrain to the 3-Hz FM stimulation. Building on predictions from unimodal studies [30–33], we were here specifically interested in the cross-modal influences of the continuous 3-Hz FM auditory stimulation, occurring independently of any transient changes in stimulus energy. We tested whether the perceptually varying auditory stimulus would lead to rhythmic modulation of visual perception, and sought evidence for rhythmic entrainment of neural activity in visual brain areas that could account for such rhythmic modulation of visual perception.

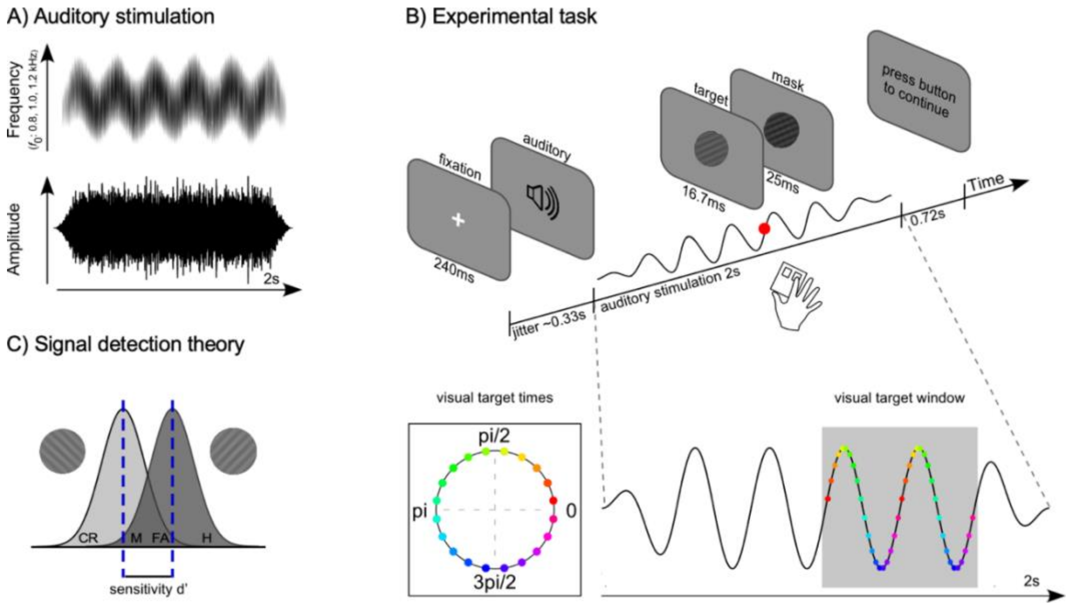

Figure 1. FM-sound characteristics, experimental task, and illustration of signal detection theory. A) Auditory stimulation. Driving stimulus characteristics of the 3-Hz frequency-modulated (FM) stimulation. Periodicity was conveyed by fluctuations in frequency, but without fluctuations in amplitude (or "stimulus energy"). The centre frequency f_0 was randomized from trial to trial and could take on one of three values: 800 Hz, 1000 Hz, and 1200 Hz. B) Experimental task. Schematic of a single trial. Each trial started with a fixation cross after which the auditory stimulation started. After an interval of at least 1000 ms, a single Gabor grating, oriented either 45- or 135-degrees, appeared briefly at a personalised contrast (16.7 ms) and was immediately masked (25 ms). Participants indicated the orientation of the grating via a button press. The key manipulation was that Gabor gratings were systematically presented with respect to the phase angle of the 3-Hz FM stimulation (20 visual target times in total; first visual target time set to 8°; distance between visual targets 18°). The initial phase of the auditory stimulus was varied on a trial by trial basis and could take one of four values: 0, pi/2, pi, and 3pi/2. Gabor gratings were presented after 1 s of auditory stimulation and could occur across two cycles. C) Signal detection theory. For each visual target time, we computed visual target sensitivity (d') based on the hit rate (H) from the 45-degree orientation condition and the false-alarm rate (FA) from the 135-degree orientation condition (CR: correct rejection; M: miss).

Results

Auditory rhythmic stimulation modulates visual target sensitivity

Visual target sensitivity was not stable across visual target times, but systematically co-varied with the phase of the auditory stimulation. Based on our staircasing of the visual target contrast, the mean d' calculated over all target times (target times depicted in Figure 1B) showed that participants performed the task better than chance, but far from ceiling (M = 1.09, SEM = 0.07). Critically, however, around the mean values, behavioural performance ebbed and flowed systematically according to the phase of the auditory 3-Hz FM stimulation. Figure 2A shows the behavioural data of six exemplary participants (see Supplementary Figure 1 for the data from all 28 participants). Circular-linear correlations between the 3-Hz FM stimulus phase and the visual target sensitivity values were systematically higher than would be expected by chance (t-test against 0, two-tailed: $t(27) = 9.007$, $p < 0.001$, $d = 1.702$). Even at the level of individual participants, circular-linear correlations reached significance for 21 out of 28 participants (see also Supplementary Figure 1).

While the observed coupling was highly robust, we also found considerable variability across participants in the *phase* of this cross-modal behavioural entrainment pattern – such that visual target sensitivity peaked at different phases of the 3-Hz FM signal in different participants (compare for example the green and the pink participant in Figure 2A). In fact, we found no support for a clear phase concentration of this behavioural entrainment when considering the full sample (Figure 2B; $N = 28$, Rayleigh $z = 1.785$, $p = 0.253$; $\theta = 109.8°$, $SEM = 17.8°$). However, when excluding the 7 participants for whom we did not observe significant cross-modal behavioural entrainment in the first place (circular-linear correlation p-values > 0.05; light-grey circles in Figure 2B), significant phase clustering became evident in the group (Figure 2C, $N = 21$, Rayleigh $z = 3.170$, $p = 0.040$; $\theta = 99.3°$, $SEM = 17.2°$).

Thus, despite variability in the observed phase of entrainment, cross-modal behavioural entrainment of visual target perception by the 3-Hz FM stimulation was highly robust, and could be identified in the majority of participants.

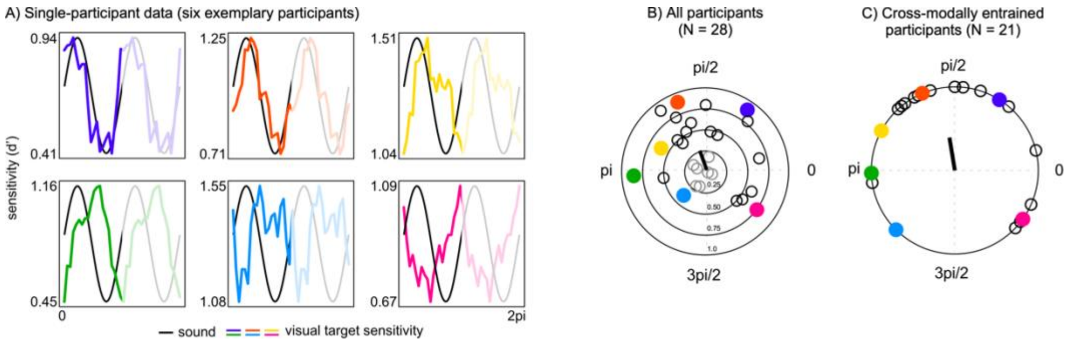

Figure 2. Rhythmic behavioural modulation of visual discrimination performance by auditory FM stimulation. A) Data from six individual representative participants. See supplementary Figure 1 for a depiction of all 28 participants. Plots show smoothed behavioural performance for all 20 visual target times (coloured lines) superimposed on a schematic of the sound (black line). Two cycles were concatenated for better visualisation purposes (2nd cycle is faded). B) Phase angle distribution of peak performance plotted as a function of cross-modal behavioural entrainment (i.e. circular-linear correlation) for all 28 participants. Colours correspond to the single-participant data as shown in A. Participants in grey did not show a significant cross-modal behavioural entrainment (circular-linear correlation: $p > 0.05$). The black arrow indicates the mean phase angle across participants. C) Phase angle distribution for $N = 21$ participants showing significant cross-modal behavioural entrainment. Data from seven participants were removed (grey circles in B). Colours correspond to the single-participant data as shown in A. The black arrow indicates the mean phase angle across participants.

Auditory FM stimulation modulates activity in auditory electrodes

We focused our EEG analyses on the 21 participants who showed significant evidence for a behavioural modulation by the 3-Hz FM stimulation. As a main indicator for neural entrainment we calculated inter-trial phase coherence (ITPC; [34]). In line with previous studies showing neural entrainment in response to a FM stimulus [30–33], we also found clear evidence for entrainment of 3-Hz activity to the FM stimulation (Figure 3B). The 3-Hz topography for ITPC values averaged over the 2.5 - 3.5 Hz frequency and 500 - 1000 ms (Figure 3A) shows a clear bilateral modulation of auditory processing with a similar distribution as previous auditory studies that also used a Laplacian transform (e.g. [35–37]). A paired-samples t-test confirmed a significant increase in ITPC in the designated auditory electrodes, relative to the pre-stimulation baseline (Figure 3B; $t(20) = 4.676$, $p < 0.001$, $d = 1.02$; $M_{\text{baseline}} = 0.05$, $SEM_{\text{baseline}} = 0.001$, $M_{\text{activation}} = 0.09$, $SEM_{\text{activation}} = 0.01$).

Auditory FM stimulation modulates activity in visual electrodes

In addition to auditory activations, the 3-Hz topography shown in Figure 3A also reveals an increase in ITPC over posterior electrodes. Such a pattern has not previously been observed in purely auditory (i.e., unimodal) studies (e.g.[35–37]) and suggests entrainment of visual processing. A paired *t*-test in canonical and a-priori-defined visual electrodes (O1, Oz, O2) confirmed a significant increase in ITPC relative to the pre-stimulation baseline (Figure 3C; *t*(20) = 2.399, *p* = 0.0263, *d* = 0.52; M_{baseline} = 0.05, SEM_{baseline} = 0.003, $M_{\text{activation}}$ = 0.07, $SEM_{\text{activation}}$ = 0.005). These data thus suggest that in our cross-modal task, the 3-Hz FM stimulation did not only entrain neural activity in auditory electrodes, but also entrained oscillatory visual activity in posterior electrodes in the absence of any continuous visual stimulation and in a fashion consistent with the cyclical pattern of visual target sensitivity in behaviour that we reported in Figure 2A.

In a supplementary analysis, we could demonstrate clear 3-Hz ITPC in visual electrodes even for trials in which the visual target occurred relatively late in the auditory stimulation (Supplementary Figure 2B) – making it unlikely that these reported effects in visual electrodes were dependent on the visual stimulation. Moreover, this analysis confirmed distinct response patterns associated with visual target processing between the selected visual and auditory electrodes. While visual target responses were evident in visual electrodes (Supplementary Figure 2B) this was much less so in auditory electrodes (Supplementary Figure 2A), thereby increasing our confidence in the separation of neural activity between the selected visual and auditory electrodes.

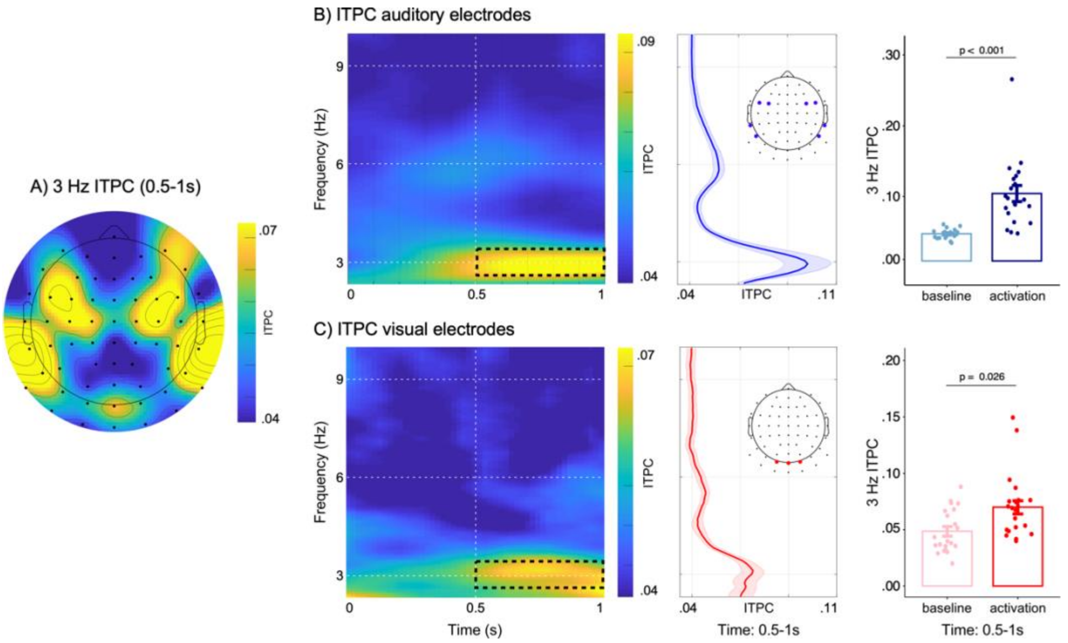

Figure 3. Entrainment of neural activity in of auditory and visual EEG electrodes. Data for *N* = 21 participants with significant behavioural cross-modal entrainment A) 3-Hz topography, averaged for the 2.5 to 3.5 Hz frequency range and 500-1000 ms time period. A surface Laplacian transform was applied to help separate contributions from auditory and visual areas. B) ITPC in auditory electrodes. Left panel shows the time-frequency representation with a clear 3-Hz activation. Black box indicates the time (500 to 1000 ms) and frequency range (2.5 to 3.5 Hz) that was used for statistical analysis. Middle panel shows ITPC values collapsed over the time window of 500-1000 ms; shaded area depicts the standard error of the mean and the inset topography depicts the electrodes used for statistical analysis. Bar plots in the right panel depict extracted 3-Hz ITPC values (2.5 to 3.5 Hz) for both, the activation period during stimulation (500 to 1000 ms; dark blue) and the pre-stimulus baseline period (-800 to -300 ms; light blue). C) ITPC in visual electrodes. Time-frequency representation of ITPC values averaged across visual electrodes shows an increase in phase coherence at the 3-Hz stimulation frequency (black box indicates time and frequency range for statistical analysis). ITPC averaged over time is shown in the middle panel; shaded area shows the standard error of the mean. Right panel shows bar plots of the extracted 3-Hz ITPC values for stimulation and baseline periods.

Neural entrainment in visual electrodes is related to cyclic modulation of visual perception

Finally, we found that the degree of neural entrainment in visual electrodes was related to the degree to which visual target sensitivity fluctuated with the 3-Hz FM stimulation (Figure 4A,B).

A k-means algorithm [38] partitioned individuals who had a low (*N* = 7; cluster centre = 0.161), medium (*N* = 11, cluster centre = 0.526), or high (*N* = 10, cluster centre = 0.788) cross-modal behavioural entrainment in a purely data-driven manner. While this sorting was performed exclusively on the pattern of behavioural data, we found striking differences in the pattern of visual ITPC between the groups (Figure 4A). For example, while neural entrainment in visual electrodes was prominent in the group that also showed clear behavioural entrainment (Figure 4A, left panel), we found virtually no entrainment in visual activity in the group that also showed no clear behavioural modulation (Figure 4A, right panel; note that this group also corresponds to the 7 participants for which we could not establish a significant effect in behaviour). A contrast analysis comparing ITPC in visual electrodes across the three groups (low, medium, high) showed a significant linear trend among the means of the three groups (*F*(1,25) = 5.658, *p* = 0.025), whereby neural entrainment in visual electrodes was largest in the participant group that also showed the largest cross-modal behavioural entrainment. Arguing for the functional relevance of visual entrainment, this linear trend among the three groups was corroborated by a significant positive correlation between ITPC values in visual electrodes and cross-modal behavioural entrainment (*rho*(27) = 0.39, *p* = 0.039) across participants.

Strikingly, when running the same analyses for the neural entrainment activity in *auditory* electrodes (Supplementary Figure 3A,B) we found no linear trend among the means of the three groups (*F*(1,25) = 1.954, *p* = 0.174), nor a significant correlation (*rho*(27) = 0.22, *p* = 0.27).

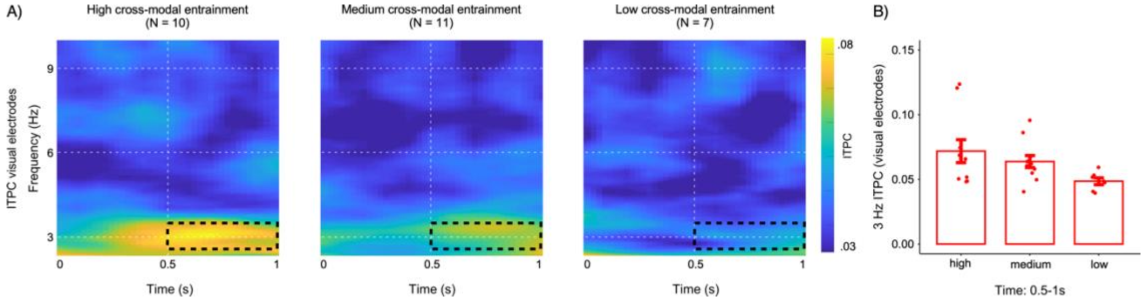

Figure 4. Neural entrainment in visual electrodes predicts the degree of cross-modal entrainment of visual perception. Data are shown for all participants (*N* = 28). A) Time-frequency maps for visual electrodes shown separately for the high, medium, and low cross-modal behavioural entrainment group. Dashed black boxes indicate the time-frequency range used for statistical analysis (2.5 - 3.5 Hz and 500 - 1000 ms). B) Red bar plots depict 3-Hz ITPC values for visual electrodes for each group.

Discussion

The current study provides a strong validation of an essential premise to the proposal that cross-modal entrainment provides useful means for organising the perception of multisensory stimulation in the natural environment [7]. Our results yielded clear behavioural evidence for cross-modal auditory-to-visual entrainment in response to a continuous FM stimulation. Further, our findings show that visual cortical activity was modulated by the 3-Hz FM stimulation in the absence of any transient changes in stimulus energy or salience in the auditory stream and without a concomitant continuous visual stimulus. Moreover, we report that the degree of cross-modal auditory-to-visual neural entrainment is related to the degree to which visual target sensitivity fluctuated with the 3-Hz FM stimulus. Together, we could demonstrate a cross-modal influence of auditory rhythmic stimulation on visual neural activity that is functionally relevant for behavioural performance.

Our study provides clear evidence for cross-modal entrainment through the careful choice of stimulus materials that remove likely alternative explanations to any rhythmic modulation of behaviour or brain activity. Building on previous work using FM stimulation in purely auditory (i.e. unimodal) settings [30–33], the constant amplitude of the FM stimulation allowed us to systematically present visual targets in relation to the phase of the auditory stimulation and thereby investigate a behavioural modulation profile that is not tied to any salient onset detections, nor potential masking effects introduced by abrupt on- or offsets. This further allowed us to overcome complications that arise when investigating neural entrainment by separating neural responses from pure evoked responses to rhythmically presented stimuli [24–27,29,39].

Nevertheless, the nature of the FM stimulus leaves open some alternative explanations that will require further investigation. While we used a FM-stimulation to avoid abrupt onset and offset effects, it might not necessarily be the case that the current findings are due to a genuine entrainment of ongoing brain oscillations. For example, participants might have perceptually “parsed” the sounds into high- and low-frequency periods resulting in evoked perceptual onsets (though the heterogeneity in the preferred “phase” of behavioural entrainment argues against any obvious “anchoring point” in the FM-sound). It is worth considering, of course, that modulation of rhythmic neural activity in accordance to changes in the properties of sensory stimuli is a natural process of information processing and need not always be discounted as artefactual. The important question in our study was whether these modulations in auditory rhythmic activity had any consequence for visual performance and visual neural activity.

The observed modulations of visual performance go beyond earlier work on rhythmic cross-modal influences. Previous studies have mainly tested on- vs. off-beat target presentations showing enhanced visual performance for targets occurring on beat with a preceding auditory rhythm [8–11]. Here, we were able to construct a behavioural modulation profile for each individual participant. Moreover, while previous studies investigating cross-modal entrainment focused either on behavioural [9,10] or neural activity [1,11] we were able to link cross-modal neural entrainment effects with behavioural performance. This link between neural entrainment of visual – but, interestingly not auditory – activity and behavioural performance reveals a clear functional relevance of the cross-modally entrained activity for behaviour.

The observed link between behavioural and neural entrainment was driven by substantial differences in the degree of entrainment across participants. One explanation might be that some participants were better able to focus solely on the visual task, and hence at ignoring the auditory stimulation. This would lead to little cross-modal entrainment of neural activity and behaviour. Another possibility is that cross-modal entrainment varies between participants for other reasons (such as hardwired anatomical connectivity), independent of potential strategic factors. In addition, we also observed heterogeneity in the preferred phase angle across participants. Previous studies using pure auditory stimulation observed similar variability across participants [30–32,40]. A possible reason for this heterogeneity is that some participants may be faster in adapting to the 3-Hz FM stimulation than others and may have different neural lags that could account for the variability [30,32,41]. Further, differences in perceptual parsing of the 3-Hz FM sound might explain some variability among the participants as well as individual difference in intrinsic brain rhythms [42].

The pattern of rhythmic modulation of EEG activity in canonical visual electrodes suggests rhythmic entrainment of visual cortical processing. Whereas one may worry that the observed visual effect merely reflects volume conduction, we have reasons to believe that the observed visual entrainment reflected more than just volume conduction. First, the increase in visual ITPC as seen in the current study, was not similarly present in purely auditory studies using a similar pre-processing pipeline and a Laplacian surface filter [35–37]. Second, our observed neuro-behavioural relationship was only significant for the ITPC in the visual electrodes, but not the auditory electrodes. If this reflected volume conduction, this correlation should have been clearer for the directly driven auditory electrodes where the neural entrainment was (not surprisingly) much larger. Third, our cycle-by-cycle analysis showed distinct activation patterns for auditory and visual electrodes.

There are multiple possible routes for auditory-to-visual entrainment. The current study does not address whether the cross-modal auditory-to-visual influences in neural activity are due to a direct influence between auditory and visual cortices as suggested by animal studies [43–45] or whether information is instead or additionally transferred indirectly through higher-order multisensory regions (i.e. superior temporal sulcus, intraparietal sulcus, and prefrontal cortex; [6,46,47]), or subcortical regions [48–50]. The temporal delay in information transfer between auditory and visual cortices – whether direct or indirect connections – and the possibility of multiple potential routes, provide a further possible explanation for the observed variability in preferred phase angles across participants.

Taken together, we have shown that a continuous auditory rhythm acts as a pacing signal by which neural oscillations can be entrained cross-modally and thereby guide visual behavioural performance ensuring that incoming visual stimuli are efficiently processed. An outstanding question is whether this tracking of environmental rhythms is special for the auditory domain, or whether, for example, a continuous visual rhythm proves equally effective to induce rhythmic modulations in the auditory domain.

Further, auditory rhythms to investigate cross-modal auditory-to-visual influences were so far restricted to the delta and theta frequency range, which conform with the range in which endogenous brain oscillations operate [1]. Whether the observed cross-modal rhythmic modulations of visual perception can operate outside of this frequency range needs to be further investigated (see also [51]). Even so, the current study provides an important addition to the cross-modal entrainment hypothesis by showing cross-modal auditory-to-visual influences on brain and behaviour – in the absence of salient stimulus on- or offsets – and with behavioural consequences for perception.

Materials and Methods

Participants

The study was approved by the Central University Research Ethics Committee of the University of Oxford and was conducted in accordance with the Declaration of Helsinki. Thirty healthy human volunteers (18 female, 12 male) participated in the study after providing written informed consent. Sample size was set a-priori based on our experience with similar tasks [32]. Data from two out of the 30 participants were discarded. One participant did not follow task instructions and pressed response buttons several times, and at random points, throughout many of the trials. The behavioural performance of the other participant was below chance (negative d' values) indicating response confusion or misunderstanding of the task. Analyses are based on the 28 remaining participants (18 female; age range = 20 to 35, M_{age} = 27.4, *SD* = 4.0). One participant was left-handed and nine participants were ambidextrous as indicated by the Edinburgh Handedness Inventory (EHI; [52]). All participants had normal or corrected-to-normal vision and reported no history of hearing, neurological, or psychiatric disorders. Participants received financial compensation of £15 per hour.

Stimuli

Auditory stimuli were generated using MATLAB software (Mathworks, Inc.). Frequency-modulated (FM) auditory stimuli were two-second narrow-band noises modulated at a rate of 3 Hz with a modulation depth of 37.5% and sampled at 48 kHz (similar to previous studies: [30,32,33]; Sound). Periodicity was conveyed via fluctuations in frequency (pitch) instead of amplitude fluctuations (see Figure 1A). Critically, this allowed us to induce a 3-Hz rhythm without changing the total energy of the auditory stimulation over time. The FM signal was faded in and out by using a 333-ms Hanning ramp, corresponding to one cycle of the 3-Hz FM stimulation. The centre frequency of the complex carrier signal was randomised from trial to trial and could take one of three values (800 Hz, 1000 Hz, 1200 Hz). The carrier signals were centred on one of these three frequencies and were constructed by adding 30 frequency components sampled from a uniform distribution with a 500-Hz range. The onset phase of the stimulus varied on a trial-by-trial basis and could take on of four values (0, pi/2, pi, and 3pi/2). All stimuli were normalised with respect to the root-mean square. Auditory stimuli were presented binaurally over EAR-Tone 3A insert earphones (3M Auditory Systems, Indianapolis, United States) at a comfortable listening level (self-adjusted by each listener).

Visual target stimuli were generated using R software (version 1.2.1335, R Core Team, 2016, Vienna, Austria). They consisted of Gabor gratings with a spatial frequency of 2.5 cycles per degree of visual angle and tilted at either 45 or 135 degrees (pi/4 and 3pi/4 respectively). Gratings had a diameter of 2 degrees visual angle and were presented foveally (screen resolution: 1920 x 1080; monitor refresh rate: 120 Hz). The masking stimulus was generated by overlaying two Gabor gratings with the same orientation as the target stimuli, either 45 or 135 degree, but with a higher spatial frequency of 10 cycles per degree of visual angle. In addition, the mask was convolved with a white Gaussian kernel. The Gaussian kernel was generated in R using the formula provided by the Visual Stimulus Generation Toolkit (Neurobehavioral Systems Inc., Albany, US)

$$f(x,y) = 2e - (\frac{\sqrt{x^2+y^2} - \mu}{\sqrt{2\sigma}})^2 - 1 \in [-1,1],$$

where the coordinates x = 0 and y = 0 correspond to the centre of the screen as well as the centre of the gaussian kernel. The parameter *μ* was constant and set to 0 and the parameter *σ* which controlled the size of the radius was set to 0.30 corresponding to a visual angle of 2 degree at a screen resolution of 1920x1080. Targets and masks were presented on a grey background (RGB: 109, 109, 109).

Critically, we manipulated when the visual targets were presented along the phase of the auditory 3-Hz FM stimulation. In particular, Gabor gratings occurred in one of 20 equally spaced times that were defined relative to the phase of the 3-Hz FM cycle of the auditory stimulation (Figure 1B: visual target times). The first phase in which a visual target could appear relative to the auditory stimulation was 8 degrees into the 3-Hz FM cycle, and subsequent targets occurred in steps of 18 degrees around the cycle. Gabor gratings were presented after a minimum of one second of the 3-Hz FM stimulation, and potential visual targets were distributed across two cycles of the auditory stimulation to reduce predictability of its exact temporal onset within the auditory stream (Figure 1B: visual target window: 1000 to 1666 ms).

To ensure accurate alignment between visual targets and the 20 possible phases of the auditory stimulus, Gabor gratings were embedded within videos with a duration of 2 seconds (240 frames), corresponding to the length of the auditory stimulation. Targets were presented for 16.7 ms (2 frames) and were immediately followed by the mask, which was presented for 25 ms (3 frames). While the contrast of the Gabor grating was individually adjusted for each participant (see Calibration procedure), the contrast of the mask was constant across participants. All other images were blank grey frames (RGB: 109,109,109). Single frames were exported to FFmpeg (http://ffmpeg.org) and converted into videos (video codec: libxvid; Video containing both the auditory stimulation and the visual target).

A second set of videos with a duration of 1 second (120 frames) were created for establishing a participant's individual Gabor contrast (see section Calibration procedure). Gabor gratings were inserted after 500 ms for 16.7ms (2 frames) and followed by mask presented for 25 ms (3 frames). The remaining frames were blank grey frames (RGB: 109, 109, 109). Single frames were subsequently exported to FFmpeg and converted into videos.

Procedure

Each session started with a calibration session to estimate the Gabor contrast threshold for each participant and was followed by a practice block before the main task started. Participants sat in a dimly lit and electrically shielded sound-attenuated booth, approximately 95 cm in front of the screen. Behavioural data were recorded online by Presentation software (version 18.3.06.02.16, Neurobehavioral Systems Inc., Albany, US). Responses were collected on a standard keyboard.

Calibration procedure. Threshold contrasts for perceiving the Gabor gratings were first titrated for each participant using a two-alternative forced choice task (2AFC). A three-down one-up rule was implemented aiming for an accuracy of ~70% [53]. In each trial, a Gabor grating was presented for 16.7 ms, tilted 45 or 135 degree, followed immediately by a mask of 25 ms duration. Participants had to indicate the orientation of the Gabor grating by pressing the right (45 degree) or left (135 degree) arrow key on the keyboard. Each trial started with a variable delay centred on 333 ms, which was followed by a white fixation cross that was presented for 240 ms. The video, containing the Gabor grating and mask, started after another variable interval (jitter centred on 333 ms) and lasted for 1000 ms. Participants were then prompted with a response screen and the next trial started after participants indicated the orientation of the Gabor grating. Participants completed three blocks of the 2AFC task, lasting about five minutes each. In each block twelve reversals were completed and the threshold contrast was determined by the average threshold of the last eight reversals (procedure similar to: [30,32]). The final threshold contrast for the Gabor gratings was defined as the arithmetic average of the individual estimates for each of the three blocks.

Cross-modal task*.* In the main task (Figure 1B for a schematic), participants had to discriminate the orientation of the Gabor gratings (45 or 135 degree). Participants were asked to listen to the auditory stimulation and to indicate the orientation of the Gabor grating as quickly as possible by pressing the right or left arrow key on the keyboard, corresponding to the 45- and 135-degree orientation respectively. Visual targets were presented for 16.7 ms at the individually established contrast and immediately masked for 25 ms. In each trial, only one visual target was presented.

The cross-modal task was self-paced, in that participants could initiate each trial on their own by pressing the space bar. After a variable delay, centred on 333 ms (1 cycle of the 3-Hz FM stimulation), a white fixation cross appeared for 240 ms. The fixation cross was followed by another variable interval centred on 333 ms after which the auditory-visual stimulation started. The auditory stimulation and the video, containing the Gabor grating and mask, started simultaneously and lasted for 2000 ms. The auditory-visual stimulation was followed by a 720 ms blank screen in which potential responses would still be counted. The participants were then prompted on the screen to initiate the next trial by pressing the space bar. Participants were explicitly instructed to maintain fixation on the middle of the screen after the fixation cross disappeared and were asked to proceed in a timely manner from trial to trial.

Participants completed a short practice block (12 trials) in which they received feedback on the screen regarding the correct identification of the Gabor orientation. No feedback was presented during the main task. In the main task, each participant completed 640 trials, resulting in 32 trials for each visual target time (16 per Gabor orientation) across the two cycles. The main task was presented in six blocks of ~10 min each with breaks of self-determined length in-between blocks and lasted on average 60 minutes (*SD* = 7 min).

After the experiment, participants completed the short version of the Speech, Spatial, and Qualities of hearing Scale (SSQ; [54]) and filled in the Edinburgh Handedness Inventory (EHI; [52]). On average each session lasted ~2.5 hours including EEG preparation.

Behavioural analysis

All statistical analyses were performed in R Studio (version 1.2.1335, R Core Team, 2016, Vienna, Austria) running the R software package (version 3.6). Circular statistics were performed by using the package ‘circular’ in R [55] and with code provided by [56] (Circular Statistics in R).

We applied signal-detection theory and calculated visual target sensitivity (d’) for each of the 20 visual target times. Trials were included in the analysis if a button press occurred between 100 and 1000 ms after the Gabor grating was presented (similar to [30–33]). Trials in which button presses occurred outside of this response window as well as trials in which no responses were made were discarded (*M* = 57 trials, *SEM* = 14.8; 8.88 ± 2.30%). In addition, trials were excluded if a participant blinked around the presentation of the Gabor grating (-500 to 100 ms), as quantified via vertical electrooculogram (*M* = 9 trials, *SEM* = 2.9; 1.46 ± 0.46%; see section EEG data acquisition and pre-processing). On average, 574 trials (*SEM* = 16.5; 89.65 ± 2.58%) were retained for the analysis of visual target sensitivity per participant.

Analysis of visual target sensitivity

For visual target sensitivity, the hit rate was defined as the percentage of 45-degree button presses in trials where a visual target with a 45-degree orientation was presented. The false alarm rate was defined as the percentage of 45-degree button presses in trials where a visual target with a 135-degree orientation was presented (see Figure 1C). For each of the 20 visual target times we calculated the sensitivity (d’) with the following equation:

$$d' = \frac{[z(H) - z(FA)]}{\sqrt{2}}$$

where *z*(H) refers to the z-score transformation of the hit rate and *z*(FA) refers to the z-score transformation of the false alarm rate. We corrected for extreme proportions (0,1) by applying the log-linear rule, adding 0.5 to both the number of hits and the number of false alarms, and 1 to both the number of 45 and 135-degree trials [57–59]. Visual target sensitivity was first calculated separately for each of the 20 visual target times. These were subsequently smoothed with an unweighted circular-moving average with a bin size of +/-2 (procedure similar to [30,32,33]).

Analysis of cross-modal behavioural entrainment

Rhythmic modulations of behavioural performance in response to FM auditory stimulation have been previously observed in pure auditory tasks [30–33]. To investigate the influence of the 3-Hz FM auditory stimulation on behavioural performance in the visual target identification task we derived three separate measures. First, we calculated a circular-linear correlation between visual target sensitivity and the phase of the 3-Hz FM stimulus at which the visual target was presented to test whether behavioural entrainment generalises to visual performance. Second, we fitted a single-cycle sine function to the behavioural data of each participant in turn. From this fit we extracted the mean performance across all 20 target times as well as the phase angle corresponding to the best behavioural performance.

Circular-linear correlations between visual target sensitivity values and the 3 Hz FM stimulus phase were calculated separately for each participant to test whether visual target sensitivity was significantly modulated by the 3-Hz FM stimulus phase (Johnson-Wehrly-Mardia Correlation Coefficient; 1000 permutations). The circular-linear correlation can be interpreted as the degree to which behavioural performance is modulated by the FM phase and we will refer to the circular-linear correlations as cross-modal behavioural entrainment throughout the manuscript. To investigate the strength of these circular-linear correlations across participants, we performed permutation testing. For each participant, we formed a permutation distribution of circular-linear correlation coefficients by shuffling the correspondence between the 3-Hz FM stimulus phase and visual target sensitivity values and calculating circular-linear correlations on each of 1000 iterations. We obtained a z-score for the actual circular-linear correlation by

$$z = \frac{(a - \mu)}{\sigma}$$

where z is the z-transformed observed data, a is the observed data (i.e., actual circular-linear correlation), and μ and σ are mean and standard deviation of the permutation distribution, respectively. The resulting z-scores were then tested against 0 using a one-sample *t*-test.

As mentioned above, we additionally fitted a single-cycle sine function to each participants' behavioural data (visual target sensitivity) using the Levenberg Marquardt nonlinear least-squares algorithm implemented in the R package minpack.lm [60]:

$$y_i \sim A\sin(2\pi f_m x \ + \ \Phi_i) + b$$

where y_i are the observed behavioural data in relation to the time steps x ε [0, 0.33] in seconds for one cycle of the f_m 3-Hz FM stimulation. A, Φ_i, and b represent the amplitude, the phase lag of the sine fit, and the intercept respectively. For each participant, we obtained the best sine-fit function $g_i(x) = A\sin(2\pi f_m x + \Phi_i)+b$ by applying the nonlinear least-squares algorithm, allowing amplitude, phase lag, and intercept to vary (three degrees of freedom). We estimated two behavioural measures from the best-fitting sine functions for each participant. First, the mean performance was estimated using the intercept of the fitted sine function and reflects the overall performance level. Second, we estimated the phase angle corresponding to peak performance by estimating the local maximum of g_i ($x_{\mathrm{max}} = \arg\max_x g_i(x)$). We obtained the phase angle in radians for peak performance by multiplying x_{max} by $2\pi f_m$, where f_m = 3 Hz for each participant. To test whether there is a systematic relation between visual performance and auditory phase across participants, optimal stimulus phases were tested for uniformity, using the Rayleigh test.

EEG data acquisition and pre-processing

EEG was acquired using Synamps amplifiers and Neuroscan acquisition software (Compumedics Neuroscan). We used a custom 62-channel setup with the following subset of electrodes of the international 10-10 system: FPz, AFz, AF3/4, AF7/8, Fz, F1/2, F3/4, F7/F8, FCz, FC1/2, FC3/4, FC5/6, FT7/8, Cz, C1/2, C3/4, C5/6, T7/8, CPz, CP1/2, CP3/4, CP5/6, TP7/8, Pz, P1/2, P5/6, P7/8, P9/10, POz, PO3/4, PO7/8, PO9/10, Oz, O1/2, Iz, I1/2. The left mastoid was used as the online reference and we included a right mastoid measurement to derive an average-mastoid reference offline. The ground electrode was placed at the left upper arm. Two bipolar electrode pairs were used to record electrooculography; one pair was placed above and below the left eye (vertical electrooculography) and another lateral of each eye (horizontal electrooculography). During acquisition, signals were low-pass filtered by an antialiasing filter (250 Hz cut-off), digitized at 1000 Hz, and stored for offline analysis.

EEG data were analysed in Matlab version 2017b (Mathworks), using a combination of EEGlab (version 14_1_2b used for pre-processing; [61]), Fieldtrip (version 20190419 used for analysis of inter-trial phase coherence; [62]), and custom scripts. For the ICA decomposition EEG raw data were first filtered offline between 1 and 40 Hz (finite impulse response filter, filter order high-pass filter: 800; filter order low-pass filter: 100), down-sampled to 500 Hz and EEG data between task blocks (i.e. during breaks) were pruned. Data were subsequently segmented into consecutive 1-s time intervals, and segments containing non-stereotypical artefacts - defined as epochs with a joint probability greater than 3 standard deviations from means of local (single-channel) and global (across channels) activity distributions - were rejected (pop_jointprob.m, locthresh & globthresh = 3). The remaining data were submitted to an independent component analysis (ICA) based on the extended Infomax [63–65]. The resulting unmixing weights were used to linearly decompose the original and down-sampled raw data and attenuate typical artefacts that reflected eye blinks, horizontal eye movements, heartbeat, and other sources of non-cerebral activity (components identified via visual inspection; *M* = 9.7, *SEM* = 0.5 components removed per data set). The code used for this pre-processing step is publicly available by [66]. The ICA-corrected raw data were subsequently filtered between 0.5 and 40 Hz (finite impulse response filter, filter order high-pass filter: 1600; filter order low-pass filter: 100)

We applied a surface Laplacian transform [67] to the EEG data as implemented by [69]. The surface Laplacian transform was applied to increase spatial resolution and to obtain a reference-free representation of the underlying current generators [36]. EEG data were epoched from -2000 to +4000 ms relative to the auditory stimulation onset and baseline corrected in the time window of -150 to 0 ms. As with the behavioural data, we only considered trials in which responses occurred within 100 to 1000 ms after visual target presentation. Trials with no button presses or responses outside of this response window were discarded. Further, we rejected all trials in which eye blinks occurred from -500 to +100 ms relative to visual target onset (*M* = 9 trials, *SEM* = 2.9; 1.46 ± 0.46%). Eye blinks were detected via vertical electrooculography prior to the ICA decomposition. In particular, trials on which the vertical EOG voltage surpassed ~200µV (approximately one-half of the maximum voltage evoked by a typical blink) were flagged and confirmed by visual inspection. Finally, epochs with an especially high variance were discarded (pop_jointprob.m, locthresh & globthresh = 5). On average 532 trials (*SEM* = 15.4; 83.15 ± 2.37%) were retained for the EEG analysis per participant.

The onset phase of the auditory stimulation varied on a trial-by-trial basis and could take one of four values: 0, pi/2, pi, and 3pi/2. In order to test for neural entrainment effects, we epoched the data relative to the rising phase of the auditory stimulation (phase 0), so that the auditory stimulus phase was consistent across trials.

EEG entrainment and statistical analysis

To investigate effects of neural entrainment in response to the auditory stimulation we calculated inter-trial phase coherence (ITPC; [34]). To this end, a fast Fourier transform was calculated, including a Hanning taper and zero padding, for each trial and each channel using a fixed number of 6 cycles across frequencies. The resulting complex numbers were normalised by dividing each complex number by its magnitude. ITPC was then calculated as the absolute value of the mean normalised complex number across trials. ITPC values can take on values between 0 (no coherence) and 1 (perfect phase coherence). ITPC was calculated for frequencies ranging from 1 to 10 Hz in steps of 0.1 Hz and in time steps of 100 ms. In an initial step, we calculated ITPC across all trials. Subsequently the analysis was repeated to determine ITPC values separately for trials in which visual targets occurred during the first (~1000 - 1333 ms) or second cycle (~1333 - 1667 ms) of the visual target window (see Figure 1B).

Statistical analyses were performed separately for electrodes associated with auditory and visual brain activity. For auditory activity, four bilateral electrodes were chosen based on the 3-Hz ITPC topography (FC3, FC5, FC4, FC6, TP7, P7, TP8, P8). The electrodes chosen correspond well with the scalp distributions of auditory generators observed in previous studies that also applied a Laplacian transform (e.g. [35]). For visual activity, we chose to use the three central occipital electrodes *a priori* (O1, Oz, O2) to investigate potential entrainment of visual activity. We focused on these canonical visual electrodes because our visual targets were presented centrally, and because these electrodes were the most remote from any possible effect of entrainment on auditory brain activity.

For statistical analyses, we extracted ITPC values for both auditory and visual electrodes at the 3-Hz stimulation frequency by calculating the average across the 2.5 to 3.5-Hz frequency window and the 500 to 1000 ms time window. The starting point of the time window was based on a previous study showing reliable auditory entrainment after 2 to 3 cycles of a 3-Hz FM stimulus [32]. The end point was chosen to avoid contamination by brain activity related to visual target onset or responding.

Paired sample *t*-tests were calculated, separately for ITPC in the selected auditory and visual electrodes, to compare the strength of peristimulus ITPC against baseline ITPC (which was defined as the average 2.5- to 3.5-Hz ITPC in the -800 to -300 ms time window before stimulation onset).

In addition, we investigated neural entrainment strength as a function of behavioural performance. We used the k-means algorithm by [38] as implemented in R (R Core Team, 2016) to cluster participants into three groups based on their cross-modal behavioural entrainment data (i.e. circular-linear correlations). K-means algorithm is an iterative algorithm that partitions the dataset into k-groups such that the sum of squares from points to the assigned cluster centre is minimised. We will refer to these three groups as high (N = 10), medium (N = 11), and low cross-modal behavioural entrainment group (N = 7). The number of participants in each group was not set a-priori but instead was defined by the clustering algorithm. After having found these groups based purely on the behavioural data, we performed a contrast analysis with the ITPC values as dependent measure to investigate whether there is a linear trend among the means of the three groups. The contrast analysis was followed up by a Spearman rank order correlation to test the relationship between behavioural and neural entrainment on a more continuous scale.

As phase coherence values are bounded between 0 and 1 and are therefore not normally distributed, ITPC values were arcsine-transformed before being submitted to statistical analysis [70]. Throughout the manuscript, effect sizes are provided as Cohens d for t-tests. All statistical tests are two-tailed and the significance level was set to $p < 0.05$ for all tests.

Data availability

The data supporting the current study are available from the corresponding author upon request and will be made available upon publication.

Acknowledgments

This research was funded by the German Research Foundation (DFG: MA 8554/1-1) to A.-K.R.B., a Marie Skłodowska-Curie Fellowship from the European Commission (ACCESS2WM) and an ERC Starting Grant from the European Research Council (MEMTICIPATION, 850636) to F.v.E., and a Wellcome Trust Senior Investigator Award (ACN) (104571/Z/14/Z) and a James S. McDonnell Foundation Understanding Human Cognition Collaborative Award (220020448) to A.C.N., and the NIHR Oxford Health Biomedical Research Centre. The Wellcome Centre for Integrative Neuroimaging is supported by core funding from the Wellcome Trust (203139/Z/16/Z). The funders had no role in study design, data collection and analysis, decision to publish or preparation of the manuscript. We also wish to thank Carsten Matke for helpful discussions and comments.

Author contributions

A.-K.R.B. and A.C.N. designed research; A.-K.R.B. performed research; A.-K.R.B., F.v.E. and A.J.Q. analysed data; A.-K.R.B., F.v.E., A.J.Q., and A.C.N. wrote the paper.

Declaration of Interests

The authors declare no competing interests.

References

1. Lakatos, P., Karmos, G., Mehta, A.D., Ulbert, I., and Schroeder, C.E. (2008). Entrainment of neuronal oscillations as a mechanism of attentional selection. Science *320*, 110–3.
2. Thut, G., Schyns, P.G., and Gross, J. (2011). Entrainment of perceptually relevant brain oscillations by non-invasive rhythmic stimulation of the human brain. Front. Psychol. *2*, 170.
3. Pikovsky, A., Rosenblum, M., and Kurths, J. (2003). Synchronization: A Universal Concept in Nonlinear Sciences. Cambridge Nonlinear Sci. Ser. 12, 432.
4. Keil, J., and Senkowski, D. (2018). Neural Oscillations Orchestrate Multisensory Processing. Neuroscientist *24*, 609–626.
5. Bauer, A.-K.R., Debener, S., and Nobre, A.C. (2020). Synchronisation of Neural Oscillations and Cross-modal Influences. Trends Cogn. Sci. *24*, 481–495.
6. Van Atteveldt, N., Murray, M.M., Thut, G., and Schroeder, C.E. (2014). Multisensory integration: Flexible use of general operations. Neuron *81*, 1240–1253.
7. Lakatos, P., Gross, J., and Thut, G. (2019). A New Unifying Account of the Roles of Neuronal Entrainment. Curr. Biol. *29*, R890–R905.
8. Simon, D.M., and Wallace, M.T. (2017). Rhythmic Modulation of Entrained Auditory Oscillations by Visual Inputs. Brain Topogr. *30*, 565–578.
9. Barnhart, A.S., Ehlert, M.J., Goldinger, S.D., and Mackey, A.D. (2018). Cross-modal attentional entrainment: Insights from magicians. Attention, Perception, Psychophys. *80*, 1240–1249.
10. Miller, J.E., Carlson, L. a, and McAuley, J.D. (2013). When what you hear influences when you see: listening to an auditory rhythm influences the temporal allocation of visual attention. Psychol. Sci. *24*, 11–8.

11. Escoffier, N., Herrmann, C.S., and Schirmer, A. (2015). Auditory rhythms entrain visual processes in the human brain: Evidence from evoked oscillations and event-related potentials. Neuroimage *111*, 267–276.
12. Bolger, D., Trost, W., and Schön, D. (2013). Rhythm implicitly affects temporal orienting of attention across modalities. Acta Psychol. (Amst). *142*, 238–244.
13. Brochard, R., Tassin, M., and Zagar, D. (2013). Got rhythm…for better and for worse. Cross-modal effects of auditory rhythm on visual word recognition. Cognition *127*, 214–9.
14. Chow, H.M., Leviyah, X., and Ciaramitaro, V.M. (2020). Individual differences in multisensory interactions: The influence of temporal phase coherence and auditory salience on visual contrast sensitivity. Vision *4*.
15. Fiebelkorn, I.C., Foxe, J.J., Butler, J.S., Mercier, M.R., Snyder, A.C., and Molholm, S. (2011). Ready, Set, Reset: Stimulus-Locked Periodicity in Behavioral Performance Demonstrates the Consequences of Cross-Sensory Phase Reset. J. Neurosci. *31*, 9971–9981.
16. Romei, V., Gross, J., and Thut, G. (2012). Sounds reset rhythms of visual cortex and corresponding human visual perception. Curr. Biol. *22*, 807–813.
17. Mercier, M.R., Foxe, J.J., Fiebelkorn, I.C., Butler, J.S., Schwartz, T.H., and Molholm, S. (2013). Auditory-driven phase reset in visual cortex: Human electrocorticography reveals mechanisms of early multisensory integration. Neuroimage *79*, 19–29.
18. Diederich, A., Schomburg, A., and Van Vugt, M. (2014). Fronto-central theta oscillations are related to oscillations in saccadic response times (SRT): An EEG and behavioral data analysis. PLoS One *9*, 1–13.
19. Naue, N., Rach, S., Strüber, D., Huster, R.J., Zaehle, T., Körner, U., and Herrmann, C.S. (2011). Auditory Event-Related Response in Visual Cortex Modulates Subsequent Visual Responses in Humans. J. Neurosci. *31*, 7729–7736.
20. Fiebelkorn, I.C., Snyder, A.C., Mercier, M.R., Butler, J.S., Molholm, S., and Foxe, J.J. (2013). Cortical cross-frequency coupling predicts perceptual outcomes. Neuroimage *69*, 126–137.
21. Cecere, R., Rees, G., and Romei, V. (2015). Individual differences in alpha frequency drive crossmodal illusory perception. Curr. Biol. *25*, 231–235.
22. Keil, J., and Senkowski, D. (2017). Individual alpha frequency relates to the sound-induced flash illusion. Multisens. Res. *30*, 565–578.
23. Mégevand, P., Mercier, M.R., Groppe, D.M., Zion Golumbic, E., Mesgarani, N., Beauchamp, M.S., Schroeder, C.E., and Mehta, A.D. (2020). Crossmodal phase reset and evoked responses provide complementary mechanisms for the influence of visual speech in auditory cortex. J. Neurosci.
24. Haegens, S., and Zion Golumbic, E. (2017). Rhythmic facilitation of sensory processing: a critical review. Neurosci. Biobehav. Rev. *86*, 150–165.
25. Helfrich, R.F., Breska, A., and Knight, R.T. (2019). Neural entrainment and network resonance in support of top-down guided attention. Curr. Opin. Psychol. *29*, 82–89.
26. Breska, A., and Deouell, L.Y. (2017). Neural mechanisms of rhythm-based temporal prediction: Delta phase-locking reflects temporal predictability but not rhythmic entrainment. PLoS Biol. *15*, e2001665.
27. Novembre, G., and Iannetti, G.D. (2018). Tagging the musical beat: Neural entrainment or event-related potentials? Proc. Natl. Acad. Sci. U. S. A. *115*, E11002–E11003.
28. Doelling, K.B., Assaneo, M.F., Bevilacqua, D., Pesaran, B., and Poeppel, D.

(2019). An oscillator model better predicts cortical entrainment to music. Proc. Natl. Acad. Sci. *116*, 201816414.

29. Obleser, J., and Kayser, C. (2019). Neural Entrainment and Attentional Selection in the Listening Brain. Trends Cogn. Sci. *23*, 913–926.
30. Henry, M.J., and Obleser, J. (2012). Frequency modulation entrains slow neural oscillations and optimizes human listening behavior. Proc. Natl. Acad. Sci. U. S. A. *109*, 20095–100.
31. Henry, M.J., Herrmann, B., and Obleser, J. (2014). Entrained neural oscillations in multiple frequency bands comodulate behavior. Proc. Natl. Acad. Sci. U. S. A. *111*, 14935–14940.
32. Bauer, A.-K.R., Bleichner, M.G., Jaeger, M., Thorne, J.D., and Debener, S. (2018). Dynamic phase alignment of ongoing auditory cortex oscillations. Neuroimage *167*, 396–407.
33. Henry, M.J., Herrmann, B., Kunke, D., and Obleser, J. (2017). Aging affects the balance of neural entrainment and top-down neural modulation in the listening brain. Nat. Commun. *8*, 15801.
34. Lachaux, J.P., Rodriguez, E., Martinerie, J., and Varela, F.J. (1999). Measuring phase synchrony in brain signals. Hum. Brain Mapp. *8*, 194–208.
35. Jaeger, M., Bleichner, M.G., Bauer, A.-K.R., Mirkovic, B., and Debener, S. (2018). Did You Listen to the Beat? Auditory Steady-State Responses in the Human Electroencephalogram at 4 and 7 Hz Modulation Rates Reflect Selective Attention. Brain Topogr. *31*, 811–826.
36. Kayser, J., and Tenke, C.E. (2015). Issues and considerations for using the scalp surface Laplacian in EEG/ERP research: A tutorial review. Int. J. Psychophysiol. *97*, 189–209.
37. SanMiguel, I., Widmann, A., Bendixen, A., Trujillo-Barreto, N., and Schröger, E. (2013). Hearing silences: human auditory processing relies on preactivation of sound-specific brain activity patterns. J. Neurosci. *33*, 8633–9.
38. Hartigan, J.A., and Wong, M.A. (1979). Algorithm AS 136: A K-Means Clustering Algorithm. Appl. Stat. *28*, 100.
39. Daume, J., Wang, P., Maye, A., Zhang, D., and Engel, A.K. (2021). Non-rhythmic temporal prediction involves phase resets of low-frequency delta oscillations. Neuroimage *224*, 117376.
40. Henry, M.J., and Obleser, J. (2013). Dissociable neural response signatures for slow amplitude and frequency modulation in human auditory cortex. PLoS One *8*, e78758.
41. Besle, J., Schevon, C.A., Mehta, A.D., Lakatos, P., Goodman, R.R., McKhann, G.M., Emerson, R.G., and Schroeder, C.E. (2011). Tuning of the Human Neocortex to the Temporal Dynamics of Attended Events. J. Neurosci. *31*, 3176–3185.
42. Kösem, A., Gramfort, A., and van Wassenhove, V. (2014). Encoding of event timing in the phase of neural oscillations. Neuroimage *92*, 274–84.
43. Lakatos, P., O'Connell, M.N., Barczak, A., Mills, A., Javitt, D.C., and Schroeder, C.E. (2009). The Leading Sense: Supramodal Control of Neurophysiological Context by Attention. Neuron *64*, 419–430.
44. Kayser, C., Petkov, C.I., and Logothetis, N.K. (2008). Visual modulation of neurons in auditory cortex. Cereb. Cortex *18*, 1560–1574.
45. Perrodin, C., Kayser, C., Logothetis, N.K., and Petkov, C.I. (2015). Natural asynchronies in audiovisual communication signals regulate neuronal multisensory interactions in voice-sensitive cortex. Proc. Natl. Acad. Sci. *112*, 273–278.

46. Ghazanfar, A.A., and Schroeder, C.E. (2006). Is neocortex essentially multisensory? Trends Cogn. Sci. *10*, 278–285.
47. Driver, J., and Noesselt, T. (2008). Multisensory Interplay Reveals Crossmodal Influences on “Sensory-Specific” Brain Regions, Neural Responses, and Judgments. Neuron *57*, 11–23.
48. Lakatos, P., Chen, C.-M., O’Connell, M.N., Mills, A., and Schroeder, C.E. (2007). Neuronal Oscillations and Multisensory Interaction in Primary Auditory Cortex. Neuron *53*, 279–292.
49. Hackett, T.A., De La Mothe, L.A., Ulbert, I., Karmos, G., Smiley, J., and Schroeder, C.E. (2007). Multisensory convergence in auditory cortex, II. Thalamocortical connections of the caudal superior temporal plane. J. Comp. Neurol. *502*, 924–952.
50. Cappe, C., Morel, A., and Rouiller, E.M. (2007). Thalamocortical and the dual pattern of corticothalamic projections of the posterior parietal cortex in macaque monkeys. Neuroscience *146*, 1371–1387.
51. Zalta, A., Petkoski, S., and Morillon, B. (2020). Natural rhythms of periodic temporal attention. Nat. Commun. *11*, 1–12.
52. Oldfield, R.C. (1971). The assessment and analysis of handedness: the Edinburgh inventory. Neuropsychologia *9*, 97–113.
53. Levitt, H. (1971). Transformed up-down methods in psychoacoustics. J. Acoust. Soc. Am. *49*, Suppl 2:467+.
54. Gatehouse, S., and Noble, W. (2004). The speech, spatial and qualities of hearing scale (SSQ). Int. J. Audiol. *43*, 85–99.
55. Agostinelli, C., and Lund, U. (2013). R package “circular”: Circular Statistics (version 0.4-7). URL https://r-forge.r-project.org/projects/circular/.
56. Pewsey, A., Neuhäuser, M., and Ruxton, G.D. (2013). Circular statistics in R (Oxford, UK: Oxford University Press).
57. Hautus, M.J. (1995). Corrections for extreme proportions and their biasing effects on estimated values of d′. Behav. Res. Methods, Instruments, Comput. *27*, 46–51.
58. Stanislaw, H. (1999). Calculation of signal detection theory measures. Behav. Res. Methods, Instruments, Comput. *31*, 137–149.
59. Ho, H.T., Leung, J., Burr, D.C., Alais, D., and Morrone, M.C. (2017). Auditory Sensitivity and Decision Criteria Oscillate at Different Frequencies Separately for the Two Ears. Curr. Biol. *27*, 3643-3649.e3.
60. Elzhov, T. V., Mullen, K.M., Spiess, A.-N., and Bolker, B. (2015). minpack.lm: R Interface to the Levenberg-Marquardt Nonlinear Least-Squares Algorithm Found in MINPACK, Plus Support for Bounds. R package version 1.2-0. https://CRAN.R-project.org/package=minpack.lm.
61. Delorme, A., and Makeig, S. (2004). EEGLAB: an open source toolbox for analysis of single-trial EEG dynamics including independent component analysis. J. Neurosci. Methods *134*, 9–21.
62. Maris, E., and Oostenveld, R. (2007). Nonparametric statistical testing of EEG- and MEG-data. J. Neurosci. Methods *164*, 177–190.
63. Bell, A.J., and Sejnowski, T.J. (1995). An Information-Maximization Approach to Blind Separation and Blind Deconvolution. Neural Comput. *7*, 1129–1159.
64. Jung, T.P., Makeig, S., Humphries, C., Lee, T.W., Mckeown, M.J., Iragui, V., and Sejnowski, T.J. (2000). Removing electroencephalographic artifacts by blind source separation. Psychophysiology *37*, 163–178.
65. Jung, T.P., Makeig, S., Westerfield, M., Townsend, J., Courchesne, E., and Sejnowski, T.J. (2000). Removal of eye activity artifacts from visual event-

related potentials in normal and clinical subjects. Clin. Neurophysiol. *111*, 1745–1758.

66. Stropahl, M., Bauer, A.-K.R., Debener, S., and Bleichner, M.G. (2018). Source-Modeling auditory processes of EEG data using EEGLAB and brainstorm. Front. Neurosci. *12*, 309.

67. Perrin, F., Pernier, J., Bertrand, O., and Echallier, J.F. (1989). Spherical splines for scalp potential and current density mapping. Electroencephalogr. Clin. Neurophysiol. *72*, 184–187.

68. Cohen, M.X. (2014). Analyzing Neural Time Series Data (MIT Press).

69. Cohen, M. (2014). Analyzing neural times series data (Cambridge, Massachusetts, London, England: MIT Press).

70. Studebaker, G.A. (1985). A “rationalized” arcsine transform. J. Speech Hear. Res. *28*, 455–62.

Supplementary Figures

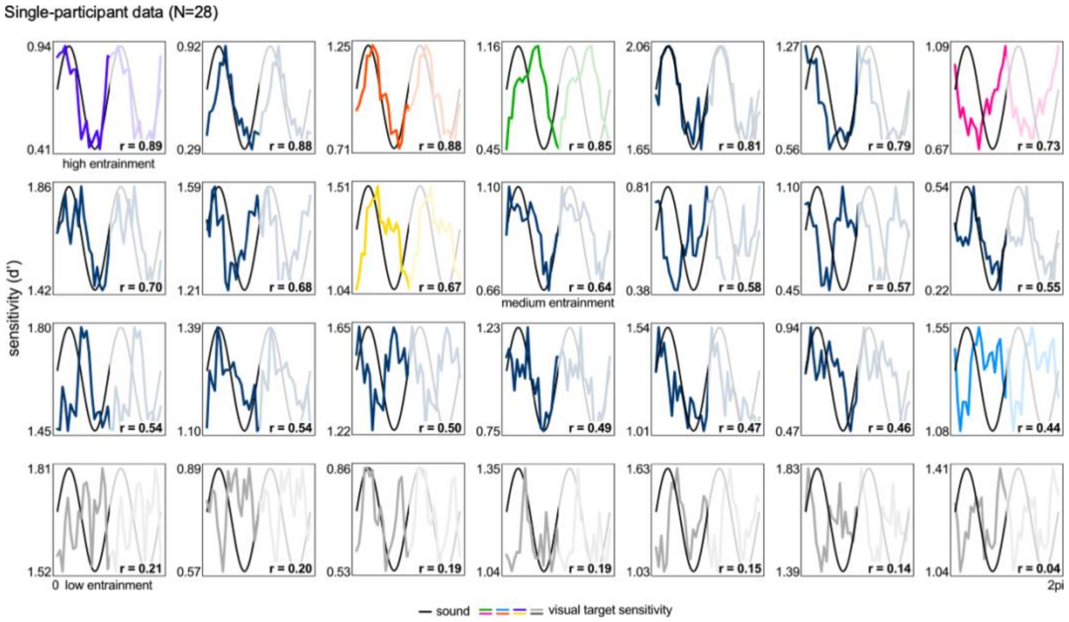

Supplementary Figure 1. Rhythmic behavioural modulation of visual discrimination performance for all participants. Single-participant data for all 28 participants ordered in descending order from high to low cross-modal behavioural entrainment (i.e. circular-linear correlation; correlation value is shown in each plot). Plots show smoothed behavioural performance for all visual target times (coloured and grey/dark blue lines) superimposed on a schematic of the sound (black line). The coloured and grey lines correspond to participants in Figure 2. Further, participants were divided into three groups: high (N = 10), medium (N = 11), and low cross-modal behavioural entrainment (N = 7) group. Groups were based on k-means clustering and used for the analysis of the neuro-behavioural relationship (see Figure 4 and Supplementary Figure 3).

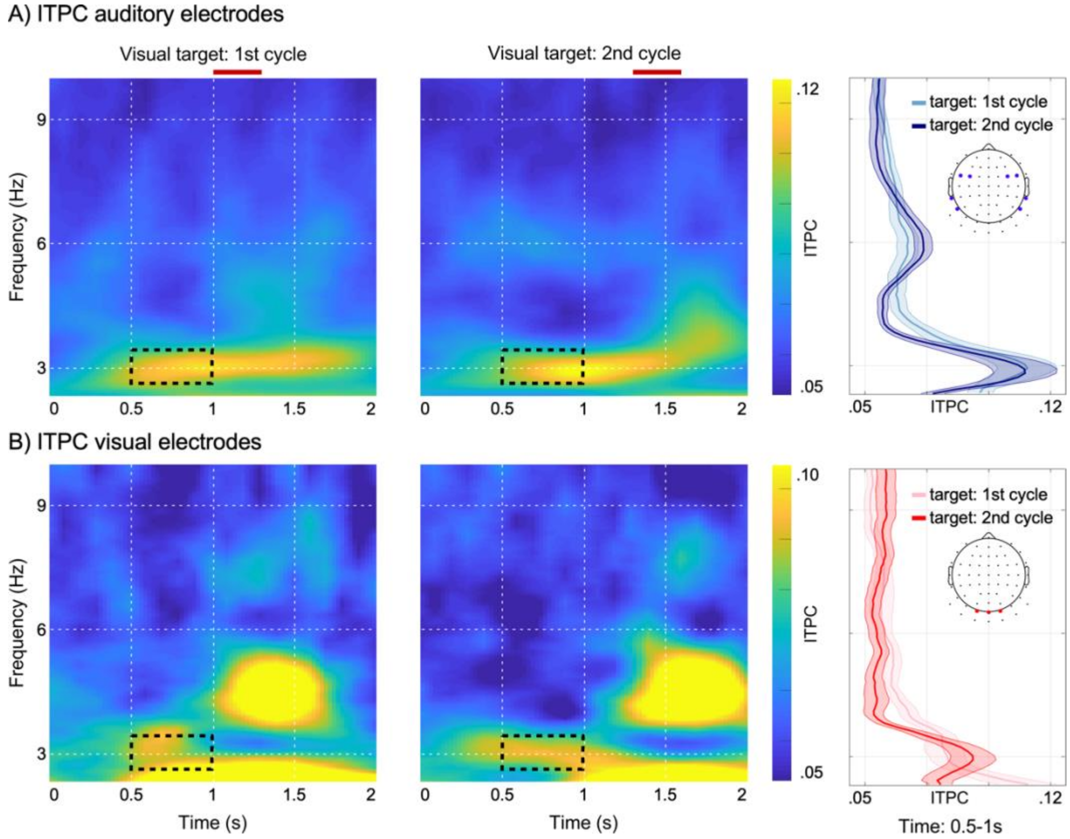

Supplementary Figure 2. Entrainment of neural activity in auditory and visual EEG electrodes separated by target occurrence. ITPC analysis separately for visual targets occurring during first (~1000 to 1333 ms) or second cycle (~1333 to 1667 ms) of the visual target window (N = 21 participants are shown; see Figure 1B for visual target window). Visual target windows are indicated via red bars on top of the time-frequency representations. A) ITPC in auditory electrodes: left and middle panel show time-frequency representations for the first and second cycle of the visual target window. Right panel shows ITPC values collapsed over time (500 - 1000 ms) separately for targets occurring during the first (light blue) or second cycle (dark blue); shaded areas depict the standard error of the mean and the inset topography depicts the electrodes used for plotting. B) ITPC in visual electrodes: left and right panels show time-frequency representation of ITPC values averaged across visual electrodes for trials in which visual targets were presented in the first (left) and second (middle) cycle. ITPC averaged over the time window of 500 - 1000 ms is shown in the middle panel separately for targets occurring in the first (light red) and second cycle (dark red); shaded areas show the standard error of the mean and inset topography indicates electrodes used for plotting.

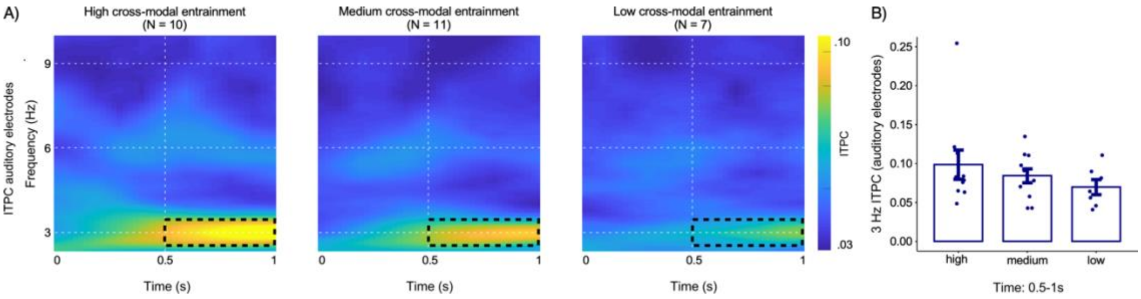

Supplementary Figure 3. Neural entrainment in visual auditory electrodes separated according to behavioural performance. A). Time-frequency representations of ITPC values for auditory electrodes plotted separately for high, medium, and low cross-modal behavioural entrainment groups. Dashed black boxes indicate the time-frequency range used for statistical analysis (2.5 - 3.5 Hz and 500 - 1000 ms). B) Bar plots (dark blue) show ITPC values for the three groups.